Propagating Waves as a Cortical Mechanism of Direction-Selectivity in V1 Motion Cells

Stewart Heitmann
University of Pittsburgh
Department of Mathematics
Pittsburgh, PA 15260.
heitmann@pitt.edu

Bard Ermentrout
University of Pittsburgh
Department of Mathematics
Pittsburgh, PA 15260.
bard@pitt.edu

ABSTRACT

The majority of neurons in primary visual cortex respond preferentially to moving bars of light with a specific orientation and direction of motion. The directional selectivity of those neurons implies that their responses cannot be achieved with separate spatial and temporal neural processes. How cortical neurons achieve non-separable space-time responses is still a mystery. We present a mathematical model of visual cortex in which neurons are predisposed to traveling waves of activity in a given anatomical direction. Those neurons resonate vigorously with moving stimuli that have a similar space-time signature to the intrinsic traveling wave. Yet they are quiescent to stimulus motion in the opposite direction. The model demonstrates how direction-selectivity can arise from the spatiotemporal properties of intrinsic cortical activity without resort to explicit time delays.

Categories and Subject Descriptors

I.2.10 [**Computing Methodologies**]: Artificial Intelligence-Vision and Scene Understanding[Perceptual reasoning]

General Terms

Theory

Keywords

Visual cortex, Receptive field, Motion detector, Traveling waves

1. INTRODUCTION

Most neurons in primary visual cortex respond selectively to the speed and direction of moving stimuli [13, 12]. A minority of those cells respond to stimuli that have separate light and dark regions in time and space. These neurons are said to have separable space-time receptive fields and their responses can be explained by the product of independent spatial and temporal neural processes [1, 6]. However directionally-selective responses cannot be separated in space and time. Instead, the spatiotemporal responses of the neuron must interact in some way to produce the observed response. The neural mechanism by which that is achieved has yet to be understood.

Contemporary accounts of direction-selectivity typically rely on spatially graded time delays, either in the relay cells of the lateral geniculate nucleus [19, 18] or in the dendritic arbors of the cortical cells [15, 3]. We propose a different approach in which the cortical neurons are predisposed to generate propagating waves of activity that consistently follow a given anatomical direction. The preferred direction of the intrinsic wave interacts with that of the stimulus to produce a directionally-selective cortical response.

Specifically, we present a one-dimensional neural field model of visual cortex with Wilson-Cowan dynamics [21, 22] and non-local Gaussian connection densities. We show that small spatial shifts in the excitatory connections are sufficient to induce intrinsic waves of activity that consistently propagate in one direction. We then use moving sinusoidal gratings to show that stimuli which resonate with the space-time signature of the intrinsic wave produce the strongest response. Moreover, the directional sensitivity of the response is remarkably specific when competing neurons are tuned to motion in opposite directions.

2. MODEL

Visual cortex was modeled by a one-dimensional neural field comprising a single layer of inhibitory cells sandwiched between two layers of excitatory cells (Figure 1). Each cell in the model represents a local population of neurons that receives recurrent input from itself and other excitatory and inhibitory cell populations that are nearby. The activation dynamics of each cell follow that of the Wilson-Cowan model [21, 22]. Specifically, the integro-differential equations were defined as,

$$\tau_e \dot{U}_e = -U_e + F_e(V_e + J) \tag{1}$$

$$\tau_i \dot{U}_i = -U_i + F_i(V_i) \tag{2}$$

$$\tau_e \dot{U}_f = -U_f + F_f(V_f + J) \tag{3}$$

where $U_e(x,t)$ and $U_f(x,t)$ represent the spatiotemporal activity of excitatory cells in the upper and lower layers respectively. Likewise, $U_i(x,t)$ represents the spatiotemporal activity of the inhibitory cells. The sigmoidal function,

$$F(V) = 1/(1+\exp(-V)) \tag{4}$$

BICT 2015, December 03-05, New York City, United States

DOI 10.4108/eai.3-12-2015.2262423

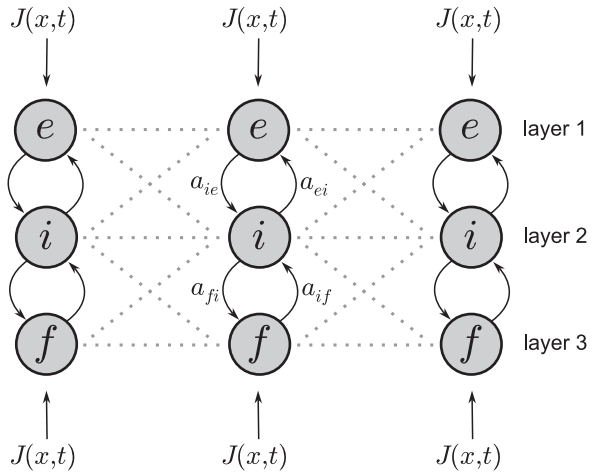

Figure 1: Schematic of the model. Cells labeled e and f are excitatory. Cells labeled i are inhibitory. $\mathbf{J(x,t)}$ represents the visual stimulus. Spatial coupling (dots) is Gaussian with distance. Coupling densities of e and f cells are weakly asymmetric such that e cells favor connections to the right and f cells favor connections to the left (asymmetry not shown). Self-connections are omitted for clarity.

Table 1: Parameters of the model.

Parameter	Description
$U_e(x,t)$	Excitatory state (layer 1)
$U_i(x,t)$	Inhibitory state (layer 2)
$U_f(x,t)$	Excitatory state (layer 3)
$J(x,t)$	Spatiotemporal stimulus
$K(x)$	Spatial coupling kernel
$\sigma_e = 0.05$	Spread of excitation (mm)
$\sigma_i = 0.15$	Spread of inhibition (mm)
$\delta_e = +0.02$	Spatial offset layer 1 (mm)
$\delta_f = -0.02$	Spatial offset layer 3 (mm)
$a_{ee} = 12$	Coupling weight (e to e)
$a_{ei} = 10$	Coupling weight (i to e)
$a_{ie} = 10$	Coupling weight (e to i)
$a_{ii} = 1$	Coupling weight (i to i)
$a_{if} = 10$	Coupling weight (f to i)
$a_{fi} = 10$	Coupling weight (i to f)
$a_{ff} = 12$	Coupling weight (f to f)
$b_e = 1.75$	Excitatory threshold
$b_i = 2.6$	Inhibitory threshold
$\tau_e = 5$	Excitatory time constant (ms)
$\tau_i = 10$	Inhibitory time constant (ms)
α	Stimulus amplitude
f_x	Spatial frequency (cycles/mm)
f_t	Temporal frequency (cycles/ms)

defines the firing rate of the cell in response to an incoming current $V(x,t)$. Visual stimulation is represented by the spatiotemporal injection current $J(x,t)$. Stimulation was applied to the excitatory cells only. Parameters τ_e and τ_i define the time constants of excitation and inhibition. All parameter values are listed in Table 1.

Cells were spatially connected according to Gaussian-with-distance connection densities and periodic boundary conditions. The cells of adjacent layers were likewise spatially connected but the upper and lower layers had no direct connections between them. The net current into each cell type was thus,

$$V_e = a_{ee}\, K_e \otimes U_e - a_{ei}\, K_i \otimes U_i - b_e \tag{5}$$

$$V_i = a_{ie}\, K_e \otimes U_e - a_{ii}\, K_i \otimes U_i + a_{if}\, K_f \otimes U_f - b_i \tag{6}$$

$$V_f = a_{ff}\, K_f \otimes U_f - a_{fi}\, K_i \otimes U_i - b_e \tag{7}$$

where the convolution operator,

$$K(x) \otimes U(x,t) = \int K(x-y)\, U(x,t)\, dy, \tag{8}$$

represents the summation of neural activity $U(x,t)$ according to the spatial coupling kernel $K(x)$. The coupling kernel describes the spatial density of axonal projections from each cell. That coupling is also weighted by cell type, such that parameter a_{ei} denotes the weight of the connection from cell type i to cell type e. Parameters b_e and b_i define the firing thresholds of excitation and inhibition, respectively.

The Gaussian coupling kernel was defined as,

$$K(x) = \frac{1}{\sigma\sqrt{\pi}} \exp\left(\frac{-(x-\delta)^2}{\sigma^2}\right), \tag{9}$$

where σ is the spatial spread of the coupling and δ is the spatial offset of the peak. The offset introduces asymmetry into the spatial coupling. Asymmetry was only applied to the excitatory projections, namely $K_e(x)$ and $K_f(x)$.

The visual stimulus was represented by a moving grating,

$$J(x,t) = \frac{\alpha}{2}\big(\cos(2\pi f_x\, x + 2\pi f_t\, t) + 1\big), \tag{10}$$

with peak amplitude α, spatial frequency f_x (cycles/mm) and temporal frequency f_t (cycles/sec).

3. RESULTS

We began by considering the dynamics of a pair of excitatory-inhibitory cells isolated from the network. The connection weights $a_{ee} = 12$, $a_{ei} = 10$, $a_{ie} = 10$ and $a_{ii} = 1$ were chosen so that the nullclines crossed at the knee of the cubic nullcline (Figure 2A). This system is known to undergo a supercritical Hopf bifurcation from a stable fixed point to a stable limit cycle when the injection current J surpasses some critical value [9]. In this case, the stable fixed point is $U_e = 0.12, U_i = 0.17$ for $J = 0$ and the critical value for limit cycles is $J_c = 0.41$. We reasoned that the supercritical Hopf was an appropriate regime for obtaining a graded neural response since the amplitude of the limit cycle rises smoothly with stimulation current. We tacitly assume that the perceptual decision is related to the peak amplitude of the oscillation in U_e.

The effects of spatial coupling were then investigated using a two-layer variant of the model in which the spatial coupling kernels $K(x)$ were retained but the $U_f(x,t)$ cells were disconnected from the network ($a_{if} = a_{fi} = 0$). This variant is equivalent to a conventional ring of Wilson-Cowan excitatory-inhibitory cells except for the asymmetric spatial coupling in $K_e(x)$. The spatial footprints of $K_e(x)$ and $K_i(x)$

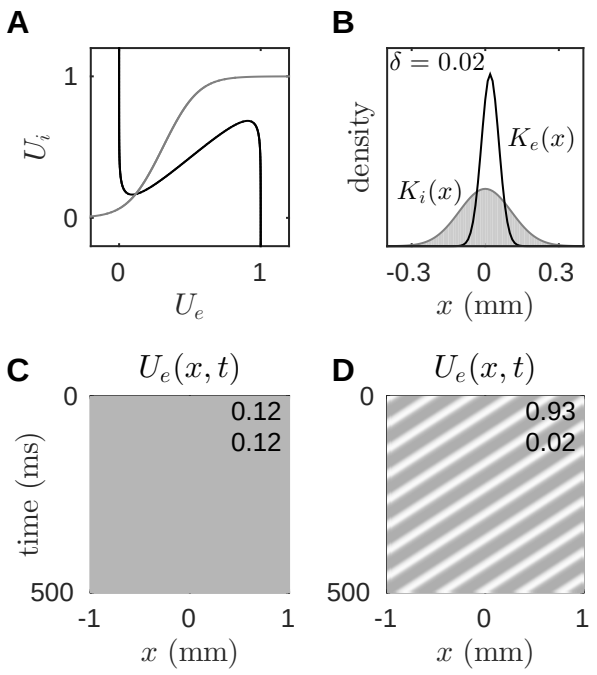

Figure 2: Directed traveling waves in the two-layer variant of the model ($\mathbf{a_{if} = a_{fi} = a_{ff} = 0}$). (A) Nullclines of an isolated pair of excitatory-inhibitory cells for $\mathbf{J = 0}$. (B) Gaussian spatial coupling kernels. The peak of $\mathbf{K_e(x)}$ is offset from $\mathbf{x = 0}$ by $\delta = \mathbf{0.02}$ mm. (C) Space-time plot of $\mathbf{U_e(x,t)}$ for $\mathbf{J = 0}$. The system is quiescent. (D) Space-time plot of $\mathbf{U_e(x,t)}$ for $\mathbf{J = 1.2}$. Waves occur intrinsically and propagate leftwards. Color scale ranges from dark gray ($\mathbf{U_e = 0}$) to white ($\mathbf{U_e = 1}$). Minimum and maximum values are listed in the top-right corner of each space-time plot.

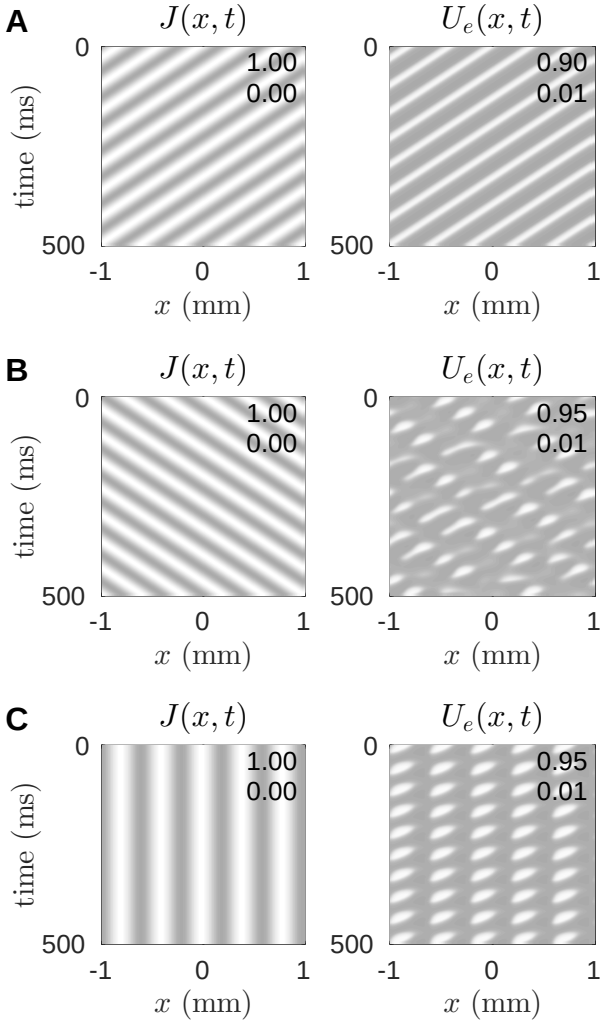

Figure 3: Space-time responses of the two-layer model to moving sinusoidal gratings. Stimuli are shown on the left, $\mathbf{J(x,t)}$. Responses are on the right, $\mathbf{U_e(x,t)}$. Dark gray represents 0. White represents 1. Minimum and maximum values are listed in the corners. (A) Case of a leftwards moving grating that matches the intrinsic wave dynamics ($\alpha = \mathbf{1}, \mathbf{f_x = 2.5}, \mathbf{f_t = 15}$). (B) Case of a rightwards moving grating ($\alpha = \mathbf{1}, \mathbf{f_x = 2.5}, \mathbf{f_t = -15}$). (C) Case of a stationary grating ($\alpha = \mathbf{1}, \mathbf{f_x = 2.5}, \mathbf{f_t = 0}$).

were chosen to span less than 0.6 mm anatomical distance (Figure 2B) which is consistent with the span of pyramidal dendrites [20]. The spread of inhibitory coupling ($\sigma_i = 0.15$ mm) was chosen to be three times broader that of the excitatory coupling ($\sigma_e = 0.05$ mm) since broad inhibition is known to induce intrinsic wave formation in neural fields [2, 11]. The spatial shift $\delta = 0.02$ mm applied to the excitatory coupling density was chosen arbitrarily.

The two-layer model produced no spatiotemporal response to zero stimulation (Figure 2C). Yet it produced intrinsic traveling waves under constant uniform stimulation (Figure 2D). Furthermore, those waves consistently propagated in the opposite direction of the spatial shift applied to the excitatory spatial coupling. In this case, the waves traveled leftwards in response to a rightward shift in $K_e(x)$. We conjectured that this directional bias in the intrinsic wave dynamics could be exploited by cortex to achieve directional selectivity in visual motion detection.

It was hypothesized that the network would respond maximally to moving sinusoidal gratings (equation 10) that best matched the spatiotemporal frequencies of the intrinsic wave ($f_x = 2.5$ cycles/mm, $f_t = 15$ Hz). Indeed, the two-layer model did respond vigorously to the matching stimulus (Figure 3A). However, it also responded vigorously to gratings that moved in the opposite direction (Figure 3B) as well as stationary gratings (Figure 3C). Note that the responses to the non-preferred stimuli have qualitatively different space-time signatures from that of the preferred stimulus. Nonetheless, the peak responses of $U_e(x,t)$ were equally large in all cases (0.90, 0.95, 0.95). We concluded that the two-layer model was insufficient for motion discrimination since it lacked a mechanism to suppress responses to non-preferred stimuli.

The full three-layer model was proposed to overcome this

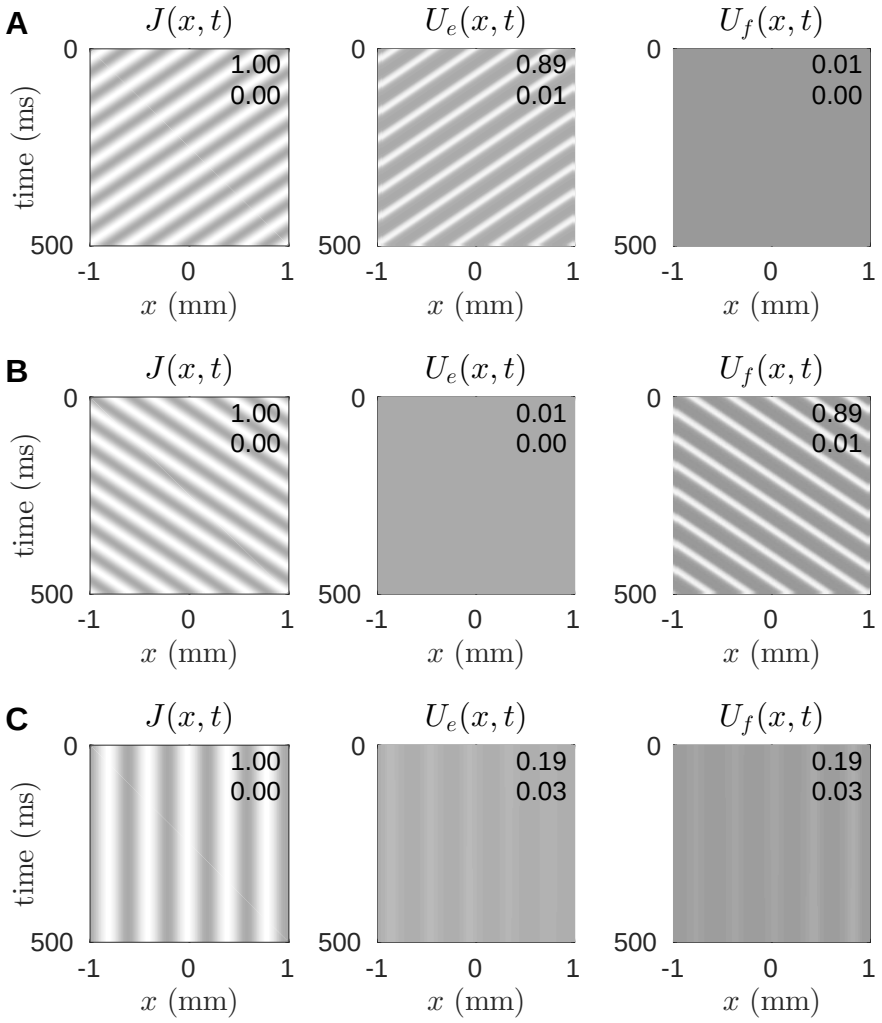

Figure 4: Direction-selective space-time responses in the three-layer model. Stimuli are shown on the left, $\mathbf{J(x,t)}$. Responses are on the right, $\mathbf{U_e(x,t)}$ and $\mathbf{U_f(x,t)}$. The $\mathbf{U_e}$ cells are tuned to respond to leftwards motion whereas the $\mathbf{U_f}$ cells are tuned to rightwards motion. Competition between these cells significantly enhances the directional selectivity of the responses. (A) Case of a leftward moving grating eliciting a strong response in $\mathbf{U_e(x,t)}$ and nil response in $\mathbf{U_f(x,t)}$. (B) Case of a rightward moving grating eliciting nil response in $\mathbf{U_e(x,t)}$ and a strong response in $\mathbf{U_f(x,t)}$. (C) Case of a stationary grating eliciting simultaneously suppressed responses in both $\mathbf{U_e(x,t)}$ and $\mathbf{U_f(x,t)}$.

limitation by having two opposing motion detector mechanisms (layers 1 and 3) which compete for dominance via the common layer of inhibitory cells. The two excitatory layers were biased towards opposing directions of motion by spatial shifting the coupling kernels $K_e(x)$ and $K_f(x)$ in equal and opposite directions ($\delta_e = +0.02$ mm, $\delta_i = -0.02$ mm). The reciprocal connections of both excitatory layers were equally weighted ($a_{ei} = a_{fi}$, $a_{ie} = a_{if}$, $a_{ee} = a_{ff}$). It was hypothesized that the excitatory layer which resonated best with the incoming stimulus would dominate the entire network response.

We tested the response of the model to moving sinusoidal gratings $J(x,t)$ that were applied equally to both $U_e(x,t)$ and $U_f(x,t)$. The three-layer model responded to the direction of motion with remarkable specificity (Figure 4). Leftwards moving gratings (panel A) elicited a strong response in $U_e(x,t)$ and virtually nil response in $U_f(x,t)$. Whereas rightwards moving gratings (panel B) elicited the opposite outcome, namely nil response in $U_e(x,t)$ and a strong response in $U_f(x,t)$. Stationary gratings (panel C) elicited subdued responses in both $U_e(x,t)$ and $U_f(x,t)$.

These findings were verified with stimuli drawn from a range of spatiotemporal frequencies (Figure 5). The tuning curves of $U_e(x,t)$ and $U_f(x,t)$ show dramatic discrimination for temporal frequencies in the 5–28 Hz band (panel A). Negative temporal frequencies correspond to leftward motion and the spatial frequency of the grating was fixed at $f_x = 2.5$ cycles/mm. By varying the spatial frequency while holding the temporal frequency fixed at $f_t = 15$ Hz — the preferred frequency for $U_e(x,t)$ — we also observed distinct spatial

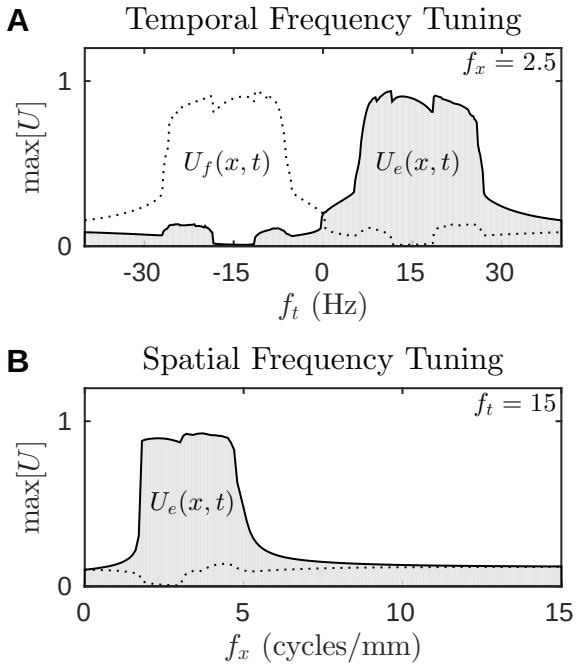

Figure 5: Tuning curves of $\mathbf{U_e(x,t)}$ (shaded) and $\mathbf{U_f(x,t)}$ (dotted) for sinusoidal moving gratings. (A) Tuning responses to gratings with a range of temporal frequencies $\mathbf{f_t \in [-40, 40]}$ Hz and a fixed spatial frequency of $\mathbf{f_x = 2.5}$ cycles/mm. Negative temporal frequencies correspond to leftward motion. (B) Tuning responses to gratings with spatial frequencies in the range $\mathbf{f_x \in [0, 15]}$ cycles/mm. The temporal frequency was fixed at the preferred frequency for $\mathbf{U_e(x,t)}$, namely $\mathbf{f_t = 15}$ Hz.

tuning in $U_e(x,t)$ for stimuli spanning 1.7–5.0 cycles/mm (panel B). The response of $U_f(x,t)$ (dotted line) was always attenuated to this stimulus because it was tuned to the opposite direction of motion ($f_t = -15$ Hz).

4. ANALYSIS

To gain insight into the selectivity of the three-layer model, we analyzed the dynamics of an isolated assembly of e-i-f cells in which the injection currents to the excitatory cells (J_e and J_f) were independent. Disparities between J_e and J_f were assumed to reflect disparities in the spatiotemporally filtered input to the opposing cell layers in the full model.

In the case of ambiguous stimuli ($J_e = J_f$) the opponent cells have symmetric solutions (U_e and U_f) for all values of J. Hence we restricted our analysis to U_e and inferred U_f by symmetry. The bifurcation structure of U_e (Figure 6A) was obtained by varying the amplitude of the ambiguous stimulus from $J = 0$ to $J = 2$. Only one stable fixed point exists for $J < 0.99$ wherein the solutions to U_e and U_f are identical. These solutions represent the quiescent responses of the opponent cells to weak stimuli.

The monostable fixed point undergoes a pitchfork bifurcation (labeled BP in Figure 6A) at $J = 0.99$ which yields

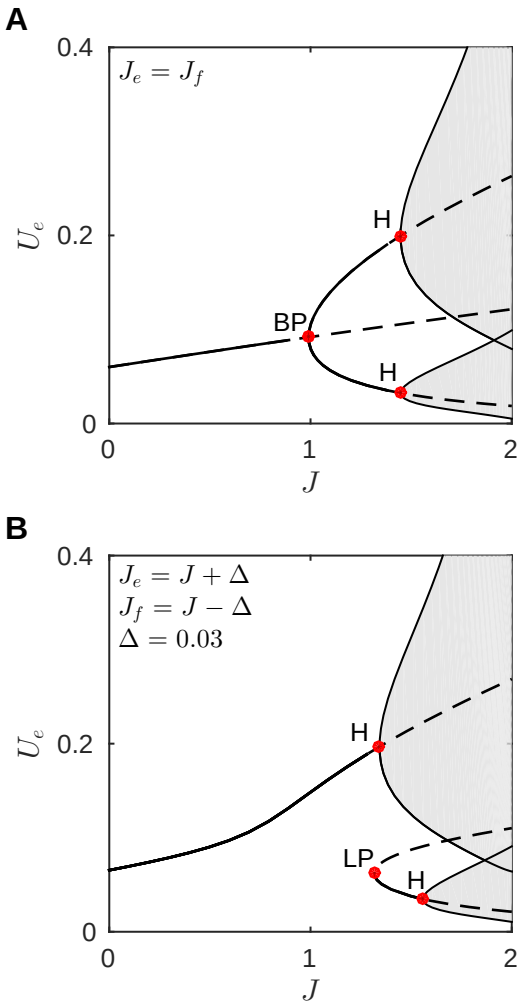

Figure 6: Bifurcation maps of an isolated assembly of *e-i-f* cells with independent stimulation $\mathbf{J_e}$ and $\mathbf{J_f}$ applied to the *e* and *f* cells. (A) Case of an ambiguous stimulus ($\mathbf{J_e = J_f}$). (B) Case of a non-ambiguous stimulus ($\mathbf{J_e \neq J_f}$) with a fixed the discrepancy $\mathbf{\Delta}$ between $\mathbf{J_e}$ and $\mathbf{J_f}$. Solid lines indicate stable solutions. Dashed lines are unstable solutions. Shaded regions indicate limit cycles. BP is branch point. H is Hopf point. LP is limit point.

a pair of stable fixed points and one unstable fixed point. By symmetry, the upper branch of fixed points in U_e corresponds to the lower branch of fixed points in U_f, and vice versa. The fate of this bistable regime is determined by initial conditions, with either fixed point being an equally likely outcome of the ambiguous stimulus. Despite their diverging values, these fixed points still represent quiescent responses because the limit cycles that drive the propagating wave have not yet appeared.

Co-existing limit cycles emerge simultaneously from each Hopf point (labeled H in Figure 6A) when the amplitude of the ambiguous stimulus reaches $J = 1.45$. The large amplitude limit cycle in U_e (upper shaded region) corresponds

to the low amplitude cycle in U_f (lower shaded region) and vice versa. The co-existing limit cycles represent the competing perceptual decisions whereby the cell with the largest limit cycle represents the winner. The fate of the system is still determined by initial conditions, with either limit cycle being an equally likely outcome for an ambiguous stimulus.

In the case of non-ambiguous stimuli ($J_e \neq J_f$) the symmetry of the system was readily broken by introducing a small disparity $\Delta = 0.03$ in the stimulation received by the opposing cells (Figure 6B). Specifically, we set $J_e = J + \Delta$ and $J_f = J - \Delta$ and varied the common stimulus strength J while holding Δ fixed. This non-symmetric system has a branch of monostable fixed points for low values of J, similar to that of the symmetric system. However the monostable fixed points do not diverge via a pitchfork bifurcation. Instead, a second branch of solutions emerges via a fold bifurcation (labeled LP) at $J = 1.32$. Immediately beyond this point, the system is in a bistable regime with a pair of co-existing stable fixed points and one unstable fixed point.

Further increases in J cause the emergence of limit cycles on both the upper and lower branches, as was the case for ambiguous stimuli, but the Hopf points (H in Figure 6B) no longer occur simultaneously. Instead, the large limit cycle emerges at $J = 1.34$ whereas the small limit cycle emerges at $J = 1.56$. The two limit cycles are no longer equally likely outcomes. For stimuli that fall between the two Hopf points ($1.34 < J < 1.56$) the possible outcomes are restricted to one limit cycle and one stable fixed point. In this case, the limit cycle corresponds to a traveling wave in the e cell layer of the full model and the fixed point represents a quiescent response in the opponent f cells. The perceptual decision is thus unambiguous even though the disparity in J_e and J_f is very small.

For larger amplitude stimuli ($J > 1.56$) the non-ambiguous stimulus evokes two stable limit cycles (shaded regions in Figure 6B) that compete for dominance. Either limit cycle could potentially win the competition, depending on initial conditions. Thus an incorrect perceptual decision is possible for strong stimuli that are weakly non-ambiguous. Greater discrepancies between J_e and J_f cause greater separation between the Hopf points thereby making a false decision less likely. Even so, false decisions rarely seem to arise from random initial conditions. So the basin of attraction for the false decision appears to be small. Furthermore, the resting state is always in the basin of attraction of the cell that receives the greater stimulation. So it is likely that a non-ambiguous stimulus applied to the resting system will inevitably converge to the correct attractor.

5. DISCUSSION

Our model demonstrates that neurons in visual cortex can potentially exploit spatiotemporal biases in the intrinsic cortical activity to successfully discriminate the direction of stimulus motion. The proposed mechanism does not require explicit time delays in neural transmission. It instead relies on collective wave formation to predispose the cortical activity to resonate with stimuli with a given space-time signature. As a consequence, any cell that is isolated from its network will lose its direction selectivity.

The formation of waves in our model arises from lateral inhibition ($\sigma_i = 3\sigma_e$) which is known to evoke intrinsic wave activity in neural fields. The directional preference of those waves arises from asymmetries in the lateral connectivity. That asymmetry need not be large. In our case, excitation was only shifted by $\delta = 0.02$ mm yet it produced consistent wave propagation in the opposite direction of the shift. The magnitude of that shift was chosen arbitrarily. Larger shifts induce faster propagating waves, hence the network can be tuned to any given stimulus speed.

Nonetheless, we find that the formation of directed propagating waves is not enough. Stimuli which propagate in non-preferred directions can also resonate with the intrinsic wave to produce strong albeit irregular peak responses. We overcame this problem by arranging the network so that waves of opposite directions compete for activation. Opponency is a common principle in sensory systems and in the present model it dramatically improved the direction-selectivity of the responses. The tuning curves of the opposing cells were mutually exclusive and exhibited sharp cut-offs in both the temporal and spatial frequency bands.

Analysis revealed that excitatory cells which compete for dominance via a common inhibitory cell are highly sensitive to discrepancies in the input currents they receive. Even small discrepancies in the inputs can greatly influence the outcome. For weak stimulation, all cells are quiescent. This represents the null response. For moderate stimulation, the excitatory cell receiving the most stimulation will oscillate robustly (as does the inhibitory cell) while the opposing excitatory cell remains quiescent. This state represents a decisive perceptual decision. For strong stimulation, all cells oscillate — hence the response is less decisive — nonetheless the cell that is stimulated most has the larger oscillation amplitude. The perceptual decision can still converge to the wrong attractor but the likelihood of a false decision is reduced when stimulus ambiguity is reduced. Yet false decisions rarely seem to occur in practice, so the basin of attraction of the correct perceptual decision appears to dominate the attractor landscape.

6. CLOSING REMARKS

The suppression of competing activity in cortex through lateral inhibition [13] has become a general principle in theoretical neuroscience although the neurophysiological evidence for it is controversial. Intracellular recordings have shown that excitatory and inhibitory inputs in cat primary visual cortex are similarly tuned for orientation [4] and direction of motion [16]. The co-occurrence of excitatory and inhibitory conductances in those cells, irrespective of the stimulus, has been interpreted as evidence against lateral inhibition as a mechanism of stimulus selectivity [17]. Yet in our model, excitation and inhibition rise and fall together on each oscillation cycle despite the lateral inhibition.

Lateral inhibition in the present model is therefore not a mechanism of stimulus suppression but rather a mechanism of wave formation. It sets the spatial scale and direction of the intrinsic wave. Stimulus suppression only arises when competition is introduced between cells with differing space-time preferences. This was demonstrated with the model that included lateral inhibition but lacked opponency. Stim-

ulus specificity was weak because the intrinsic wave partly resonated with the non-preferred stimulus as well as the preferred stimulus. Introducing opponency proved to be an effective mechanism for eliminating responses to the non-preferred stimulus. Biological systems might likewise use opponency as an effective strategy for improving selectivity among imperfect sensory detectors.

We are hopeful that this distinction between lateral inhibition and stimulus suppression may shed new light on the physiological data. In particular, the present model suggests that lateral connectivity dictates the spatial properties of the intrinsic activity which, in turn, biases the tuning response of individual cells. In this view, sensory tuning arises from the collective activity rather than by individual neurons directly filtering the sensory input. Indeed, spontaneous neural activity in visual cortex has been shown to reflect the tuning response properties of the individual cells [14]. We offer the present model as a demonstration of how such intrinsic neural activity may relate to neural function.

Furthermore, the model demonstrates how non-separable space-time receptive fields can be achieved without resort to explicit time delays. All motion detectors rely on some form of temporal asymmetry [5]. In this case the temporal asymmetry derives from the spatial phase gradient in the traveling wave, which itself derives from the asymmetry in the excitatory and inhibitory lateral coupling. Hence the present motion detector essentially works by transforming coupling asymmetry into temporal asymmetry.

One limitation of the model is that each preferred stimulus requires a dedicated layer of neurons. So it is an excessively redundant method of neural computation. While it is true that cells with similar orientation preferences in visual cortex do tend to be spatially connected [10] it is not clear how well the present model would scale up to two spatial dimensions with multiple directions of motion. It seems unlikely that so many cortical neurons would be dedicated to a single perceptual task. Elucidating a mechanism by which cells can participate in a range of perceptual decisions requires further work.

7. ACKNOWLEDGMENTS

This work was funded by USA National Science Foundation (NSF) award 1219753. The bifurcation analysis was conducted using MATCONT [7] and XPPAUT [8].

8. REFERENCES

[1] J. M. Alonso and Y. Chen. Receptive Field. *Scholarpedia*, 4(1):5393, 2009.

[2] S.-i. Amari. Dynamics of pattern formation in lateral-inhibition type neural fields. *Biol Cybern*, 27(2):77–87, June 1977.

[3] J. C. Anderson, T. Binzegger, O. Kahana, K. A. C. Martin, and I. Segev. Dendritic asymmetry cannot account for directional responses of neurons in visual cortex. *Nat Neurosci*, 2(9):820–824, 1999.

[4] J. S. Anderson, M. Carandini, and D. Ferster. Orientation tuning of input conductance, excitation, and inhibition in cat primary visual cortex. *J Neurophysiol*, 84(2):909–926, 2000.

[5] A. Borst and T. Euler. Seeing Things in Motion: Models, Circuits, and Mechanisms. *Neuron*, 71(6):974–994, Sept. 2011.

[6] G. C. DeAngelis, I. Ohzawa, and R. D. Freeman. Receptive-field dynamics in the central visual pathways. *Trends Neurosci*, 18(10):451–458, 1995.

[7] A. Dhooge, W. Govaerts, and Y. A. Kuznetsov. MATCONT: a MATLAB package for numerical bifurcation analysis of ODEs. *ACM Trans Math Softw*, 29(2):141–164, 2003.

[8] B. Ermentrout. *Simulating, analyzing, and animating dynamical systems: a guide to XPPAUT for researchers and students*. Society for Industrial Mathematics, 2002.

[9] G. B. Ermentrout and D. H. Terman. *Mathematical foundations of neuroscience*, volume 35. Springer, 2010.

[10] C. D. Gilbert and T. N. Wiesel. Columnar specificity of intrinsic horizontal and corticocortical connections in cat visual cortex. *J Neurosci*, 9(7):2432–2442, 1989.

[11] S. Heitmann and G. B. Ermentrout. Synchrony, waves and ripple in spatially coupled Kuramoto oscillators with Mexican hat connectivity. *Biol Cybern*, 109(3):333–347, June 2015.

[12] G. H. Henry, P. O. Bishop, and B. Dreher. Orientation, axis and direction as stimulus parameters for striate cells. *Vision Research*, 14(9):767–777, 1974.

[13] D. H. Hubel and T. N. Wiesel. Receptive fields, binocular interaction and functional architecture in the cat's visual cortex. *J Physiol*, 160(1):106, 1962.

[14] T. Kenet, D. Bibitchkov, M. Tsodyks, A. Grinvald, and A. Arieli. Spontaneously emerging cortical representations of visual attributes. *Nature*, 425(6961):954–956, 2003.

[15] M. S. Livingstone. Mechanisms of direction selectivity in macaque V1. *Neuron*, 20(3):509–526, 1998.

[16] N. J. Priebe and D. Ferster. Direction selectivity of excitation and inhibition in simple cells of the cat primary visual cortex. *Neuron*, 45(1):133–145, 2005.

[17] N. J. Priebe and D. Ferster. Inhibition, Spike Threshold, and Stimulus Selectivity in Primary Visual Cortex. *Neuron*, 57(4):482–497, Feb. 2008.

[18] N. J. Priebe, I. Lampl, and D. Ferster. Mechanisms of Direction Selectivity in Cat Primary Visual Cortex as Revealed by Visual Adaptation. *J Neurophysiol*, 104(5):2615–2623, Nov. 2010.

[19] A. B. Saul, P. L. Carras, and A. L. Humphrey. Temporal Properties of Inputs to Direction-Selective Neurons in Monkey V1. *J Neurophysiol*, 94(1):282–294, July 2005.

[20] N. Spruston. Pyramidal neurons: Dendritic structure and synaptic integration. *Nat Rev Neurosci*, 9(3):206–221, 2008.

[21] H. R. Wilson and J. D. Cowan. Excitatory and inhibitory interactions in localized populations of model neurons. *Biophys J*, 12(1):1–24, 1972.

[22] H. R. Wilson and J. D. Cowan. A mathematical theory of the functional dynamics of cortical and thalamic nervous tissue. *Kybernetik*, 13(2):55–80, 1973.